Conductivity Control of Al-doped ZnO Thin Films Deposited by Radio Frequency Sputtering

DONG-CHEOL OH[iD]

Optoelectronic Materials and Devices Laboratory, Department of ICT Automotive Engineering, Hoseo University, Asan-si, Republic of Korea

Corresponding author: E-mail: ohdongcheol@hoseo.edu

Films made up of Al-doped ZnO (AZO) are the promising transparent conductive oxides. Hall measurements were used to investigate the effects of varying the sputtering parameters on the electrical resistivity, electron concentration and electron mobility of a series of AZO films produced by radio frequency (RF) sputtering. Increases in plasma power, chamber pressure, argon (Ar) flow rate and decreases in substrate temperature lead to the higher electrical resistance. However, all the samples exhibit a pattern in which electrical resistivities decrease with increasing annealing temperature (below 200-400 ℃) and increase (above 200-400 ℃). As the number of electrons increases, the electrical resistance decreases and *vice-versa*. The carrier compensation effect or excess carrier compensation due to the formation or annihilation of conductive defects is responsible for these shifts in the electrical characteristics. It was also found that the conductivities of the AZO films formed *via* RF-sputtering dependent on imperfections in structure such as ionized impurities and grain boundaries, as electron mobility is shown to be proportional to the electron concentration.

Keywords: Al-doped ZnO, ZnO, Electrical properties, RF-sputtering.

INTRODUCTION

The Al-doped ZnO (AZO), has again captivated awareness as a transparent conductive oxide (TCO) material for solar cell systems [1]. Indium tin oxide (ITO) has long led TCO technology because of its excellent electrical resistivity of high $10^{-5}\,\Omega$ cm and the relatively accessible synthetic techniques of sputtering systems [2-4]. However, in the transparent opto-electronics industry, which requires a vast amount of TCO, ITO has the problems of limited resource and high price, because it is composed of the rare metals indium and tin [5]. Thus, various alternatives such as AZO, graphene and PSS:PEDOT have been developed and applied to real products such as touch screen and solar cells [6-11]. AZO is accepted as an alternative in the solar cell systems that require mass production and low price, irrespective of a-Si, CdTe and CIGS [12,13]. AZO films have been fabricated mainly using vacuum technologies such as radio frequency (RF) or direct current (DC) sputtering and solution processes such as coating and spraying [6,7,12-15]. However, it was announced that an electrical and optical quality of AZO films fabricated by RF or DC sputtering are better than those of fabricated by coating and spraying; this difference

is attributed to the various impurities and defects unintentionally included during solution processes [6,7,12-15].

A broad bandgap makes AZO transparent to the vast majority of solar light and its high conductivity is comparable to that of ITO. Single-crystalline ZnO films have background electron concentrations of high 10^{16}-low 10^{18} cm^{-3} due to unintentionally generated and incorporated defects such as H, Zn$_i$ and V$_O$ [16, 17]. However, the harsh deposition conditions of heterosubstrate, which exhibits large structural mismatch with ZnO lattices and the low growth temperature, which supplies insufficient formation energy to Zn-O bonds are favourable for developing structural imperfections, facilitating the creation of various n-type defects in ZnO films [18,19]. The high conductivity of the ZnO films can be tried in various deposition ways by doping with aluminum, gallium and indium [2,13,20]. In the doped ZnO films deposited by RF-sputtering, an electrical resistivity can attain a low of $10^{-4}\,\Omega$ cm and the electron concentration can attain a low of 10^{21} cm^{-3}: In-doped ZnO films show an electrical resistivity level of 10^{-2}-$10^{-3}\,\Omega$ cm, Ga-doped ZnO films show an electrical resistivity level of 10^{-3}-$10^{-4}\,\Omega$ cm and Al-doped ZnO films show an electrical resistivity level of $10^{-4}\,\Omega$ cm [2,13]. However, compared to AZO, Ga-doped ZnO (GZO) and

In-doped ZnO (IZO) have relative difficulties in long-time stable sputtering and high-purity target fabrication because of the small melting temperature and great vapour pressure of gallium and indium elements [21,22]. This work presents a substantial data on the conductivity control as functions of RF-sputtering processing parameters in AZO films produced on glass substrates, which feature a rather high density of structural defects.

EXPERIMENTAL

Preparation of samples: AZO films were deposited on sodalime-silica glass substrates using RF-sputter. The AZO target was fixed at the composition of $ZnO:Al_2O_3 = 98:2$ wt.% (99.99%) [20]. The AZO target was an iTASCO target, which was fabricated by sintering process. Five typical sample sets were prepared as functions of plasma power (set A), chamber pressure (set B), argon flow rate (set C), substrate temperature (set D) and annealing temperature (Table-1).

TABLE-1
FIVE AZO SAMPLE SETS PREPARED IN THIS WORK

Deposition condition			
Set #	Variable	Range	Other parameters
A	Plasma power (P_{plasma})	50-200 W	$P_{chamber}$ = 10 mT F_{Ar} = 30 sccm $T_{substrate}$ = RT $t_{deposition}$ = 30 min
B	Chamber pressure ($P_{chamber}$)	1-30 mT	P_{plasma} = 100 W F_{Ar} = 30 sccm $T_{substrate}$ = RT $t_{deposition}$ = 30 min
C	Argon flow rate (F_{Ar})	15-100 sccm	P_{plasma} = 100 W $P_{chamber}$ = 10 mT $T_{substrate}$ = RT $t_{deposition}$ = 30 min
D	Substrate temperature ($T_{substrate}$)	RT-400 °C	P_{plasma} = 100 W $P_{chamber}$ = 10 mT F_{Ar} = 30 sccm $t_{deposition}$ = 30 min
Annealing condition			
A-D	Annealing temperature (T_{anneal})	RT-500 °C	F_{Ar} = 3L/min $T_{annealing}$ = 60 min

Characterization of samples: The electrical characteristics of AZO films were studied by Hall measurement and resistivity measurement by the van der Pauw method. Indium was used as the ohmic contact required for Hall and resistivity measurements. The surface structural characteristics of AZO films were studied by the atomic-force microscopy (AFM). The AZO films had a preferred orientation of *c*-axis and a textured structure irrespective of fabrication conditions [20]. The optical characteristics of AZO films were evaluated by UV-visible spectrometry. Every AZO film had transmission values beyond 80% in the visible and infrared wavelength of 400-1000 nm [20].

RESULTS AND DISCUSSION

Fig. 1 represents the electrical characteristics of set A as a parameter of plasma power (P_{plasma}) in the range of 50-200 W under the conditions of $P_{chamber}$ = 10 mT, F_{Ar} = 30 sccm, $T_{substrate}$
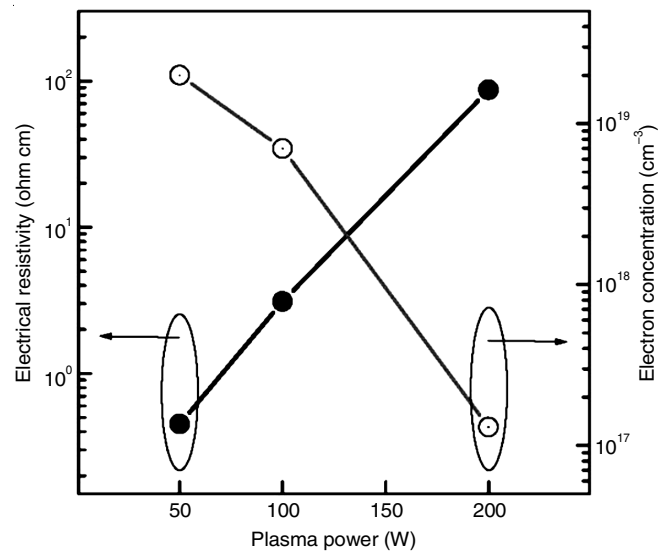
Fig. 1. Electrical resistivity *vs.* plasma power (left) and electron concentration *vs.* plasma power (right) in AZO films deposited by RF-sputtering [20]

= RT and $t_{deposition}$ = 30 min [20]. Electrical resistivity increases with the augment of P_{plasma} and electron concentration is inversely proportional to P_{plasma}. This is ascribed to the fact that the augment of P_{plasma} increases sputter yield and deposition rate, which induces carrier compensation of Al donors and donor-type defects *via* an increase of structural imperfections [23]. It is found that as the P_{plasma} augments 4 times from 50 W to 200 W, the electrical resistivity increases by two orders of magnitude as of 0.45 Ω cm to 87 Ω cm and the electron concentration decreases by two orders of magnitude as of 2×10^{19} cm^{-3} to 1×10^{17} cm^{-3} [20].

Fig. 2 represents the electrical characteristics of set B as a parameter of chamber pressure ($P_{chamber}$) in the range of 1-30 mT under conditions of P_{plasma} = 100 W, F_{Ar} = 30 sccm, $T_{substrate}$ = RT and $t_{deposition}$ = 30 min. Electrical resistivity increases with the
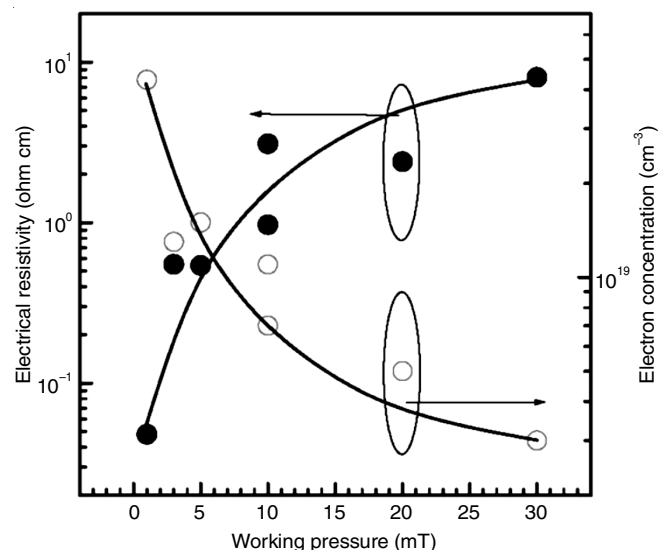
Fig. 2. Electrical resistivity *vs.* chamber pressure (left) and electron concentration *vs.* chamber pressure (right) in AZO films deposited by RF-sputtering

augment of $P_{chamber}$ and electron concentration is inversely proportional to the $P_{chamber}$. The augment of $P_{chamber}$ can be interpreted in two ways. First, it decreases the deposition rate due to the decreases of mean-free path of Ar^+ ions and of sputtered atoms, which reduces the generation of donor-type defects [24,25]. Second, it supplies the insufficient film formation energy due to impingement between sputtered atoms and Ar^+ ions, which induces the carrier compensation of the donors *via* increase of structural imperfections. The electrical characteristics of AZO films that were apparent for this work are attributed to the insufficient film formation energy. It is found that as the $P_{chamber}$ increases 30 times from 1 mT to 30 mT, the electrical resistivity increases by two orders of magnitude from 0.048 Ω cm to 8.1 Ω cm and the electron concentration decreases one order of magnitude from 4×10^{19} cm^{-3} to 3×10^{18} cm^{-3}.

Fig. 3 represents the electrical characteristics of set C as a parameter of Ar flow rate (F_{Ar}) in the range of 15-100 sccm under conditions of P_{plasma} = 100 W, $P_{chamber}$ = 10 mT, $T_{substrate}$ = RT and $t_{deposition}$ = 30 min. Electrical resistivity decreases with the augment of F_{Ar} and electron concentration is inversely proportional to the F_{Ar}. Augmenting F_{Ar} is reported to decrease the grain size and increases the number of V_O in AZO films [26,27]. It is suggested that the F_{Ar} is another factor influencing conductivity control in the AZO films; it's augment facilitates the formation of donor-type defects. It is found that as the F_{Ar} augments 7 times from 15 sccm to 100 sccm, the electrical resistivity decreases by two orders of magnitude from 12 Ω cm to 0.20 Ω cm and the electron concentration increases by one order of magnitude from 1×10^{18} cm^{-3} to 2×10^{19} cm^{-3}.
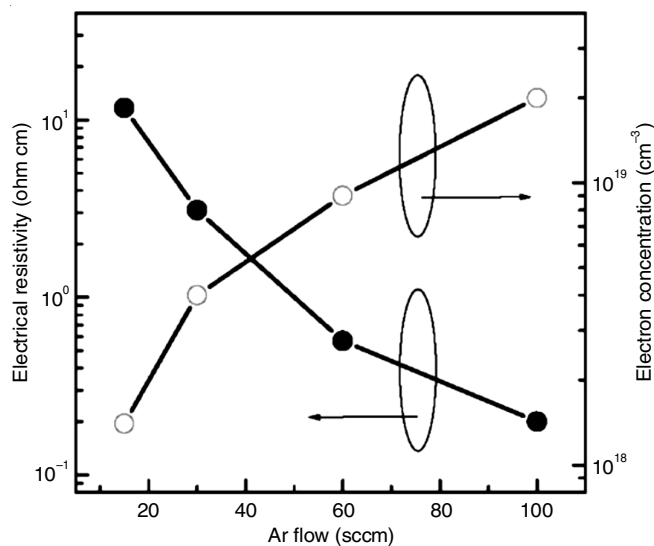
Fig. 3. Electrical resistivity *vs.* Ar flow rate (left) and electron concentration *vs.* Ar flow rate (right) in AZO films deposited by RF-sputtering

Fig. 4 represents the electrical characteristics of set D as a parameter of substrate temperature ($T_{substrate}$) in a range of RT-400 ºC under conditions of P_{plasma} = 100 W, $P_{chamber}$ = 10 mT, F_{Ar} = 30 sccm and $t_{deposition}$ = 30 min. Electrical resistivity decreases with the augment of $T_{substrate}$ and electron concentration is inversely proportional to the $T_{substrate}$. This is ascribed to the fact that the augment of $T_{substrate}$ increases the energy necessary for the
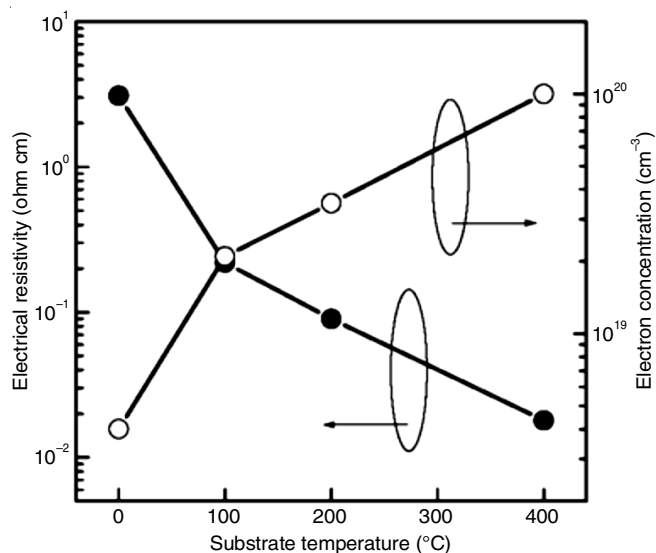
Fig. 4. Electrical resistivity *vs.* substrate temperature (left) and electron concentration *vs.* substrate temperature (right) in AZO films deposited by RF-sputtering

formation of Al-Zn-O bonds, which reduces the formation of structural imperfections and suppresses the carrier compensation of Al donors and donor-type defects [28]. It was found that as the $T_{substrate}$ augments 15 times from RT to 400 ºC the electrical resistivity decreases by two orders of magnitude as of 3.1 Ω cm to 0.018 Ω cm and the electron concentration increases by two orders of magnitude from 4×10^{18} cm^{-3} to 1×10^{20} cm^{-3}.

Fig. 5a-d represents the electrical characteristics as a parameter of annealing temperature (T_{anneal}) under an Ar ambient in the temperature range of RT-500 ºC for all deposited AZO films (sets A-D). All samples have a common trend in which, below 200-400 ºC, electrical resistivities decrease with the augments of T_{anneal} and, above 200-400 ºC, they increase with the augments of T_{anneal} and electron concentrations are inversely proportional to the T_{anneal}. The change of electrical resistivity in the AZO films originates from the carrier compensation *via* formation and annihilation of conductive defects [16,29]. It is ascribed to the fact that, below a critical temperature, the decreases of electrical resistivity with the augments of T_{anneal} are due to the suppression of carrier compensation by reduction of structural imperfections such as Zn_i. However, above the critical temperature, the increases of electrical resistivity are due to enhancement of carrier compensation by generation of structural imperfections as such as V_O [16,29]. This T_{anneal} dependence of the electrical characteristics in the region below the critical temperature is similar to the $T_{substrate}$ dependence of the electrical characteristics, which indicates that post annealing after film deposition can affect the electrical characteristics of AZO films as much as substrate heating during film deposition. It is found that in case of the sample deposited at P_{plasma} = 200 W, $P_{chamber}$ = 10 mT, F_{Ar} = 30 sccm and $T_{substrate}$ = RT, the electrical resistivity significantly decreases from 87 Ω cm to 0.037 Ω cm and the electron concentration increases from 1×10^{17} cm^{-3} to 1×10^{20} cm^{-3}, when the sample was annealed at 400 ºC. Meanwhile it was found that in the case of the sample deposited at P_{plasma} = 100 W, $P_{chamber}$ = 10 mT, F_{Ar} = 30 sccm and $T_{substrate}$ =
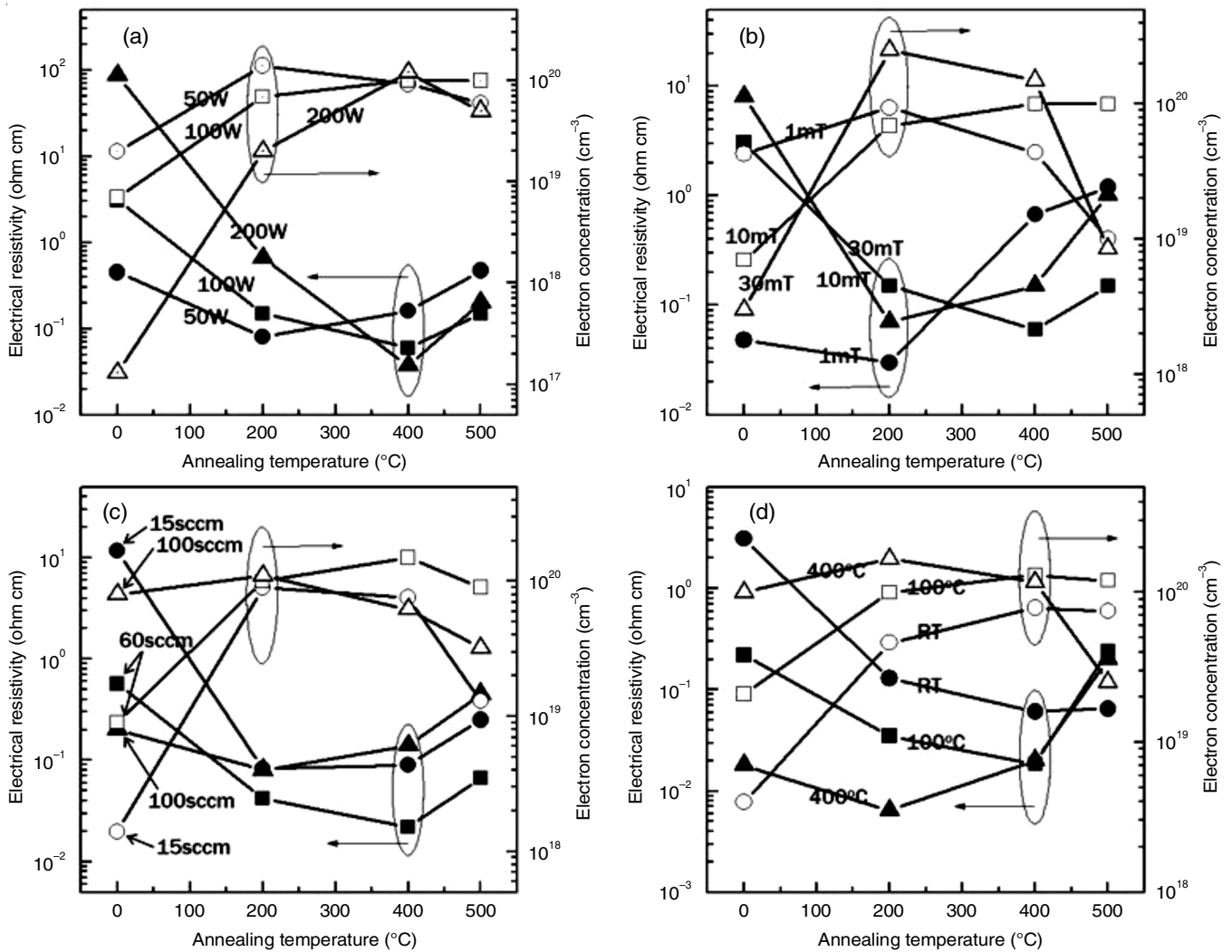
Fig. 5. Electrical resistivity *vs*. annealing temperature (left) and electron concentration *vs*. annealing temperature (right) in AZO films deposited by RF-sputtering: (a) plasma power, (b) working pressure, (c) Ar flow rate and (d) substrate temperature

400 ºC, the electrical resistivity decreases from 0.018 Ω cm to 0.0064 Ω cm and the electron concentration increases from 1 × 10^{20} cm^{-3} to 2 × 10^{20} cm^{-3}, when the sample was annealed at 200 ºC.

Fig. 6 represents the relationship of electron mobility and electron concentration in all the deposited AZO films including the annealed ones. It is important to understand that the sample with a low electron concentration has a low value of electron mobility, whereas the sample with a high electron concentration has a high value of electron mobility. This is opposite to the general electron transport mechanism of semiconductors, in which electron mobility is inverse-proportional to electron concentration, as determined by lattice scattering and defect scattering [30,31]. In case of single-crystalline compound semiconductor materials, lattice scattering consists of optical-polar phonon scattering, deformation potential scattering and piezoelectric potential scattering due to interferences of lattice phonons and defect scattering was determined by ionized-impurity scattering due to incorporated impurities [30,31].

However, in case of poly-crystalline AZO films that contain large numbers of grains and grain boundaries, defect scattering
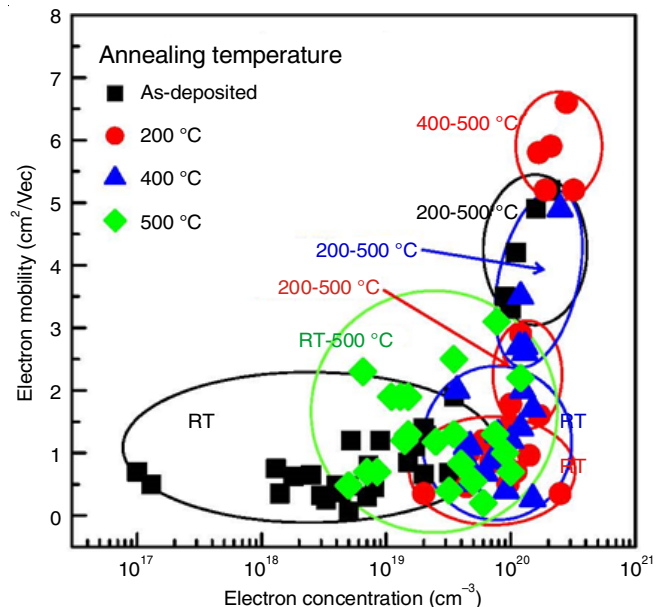
Fig. 6. Relationship of electron concentration and electron mobility for all AZO films in this work

by grain boundaries, which describes how many electrons can move through grain boundaries by field emission effect, should be included in the electron transport mechanism [13,32,33]. Also, the AZO films deposited at higher substrate temperatures have higher electron concentration and electron mobility, whose value becomes larger after annealing in an appropriate temperature range. This is ascribed to the fact that the suppression of carrier compensation by the reduction of structural imperfections simultaneously induces increase of electron concentration and increase of electron mobility. The AZO samples deposited at 400-500 ℃ and annealed at 200 ℃ are shown to have the highest values of electron concentration and electron mobility.

Conclusion

In this work, an in-depth investigation into regulating the conductive properties of RF-sputtered Al-doped ZnO (AZO) films on glass substrates is conducted. It could be summarized that all sputtering parameters had important effect with the generation and the reduction of conductive defects in AZO films, causing carrier compensation or excess carrier compensation. Even though the composition of Al in the AZO target was fixed at 2%, the electrical resistivity of AZO films increased with augments of plasma control and working pressure; however, the electrical resistivity decreased with augments of Ar flow rate and substrate temperature. The electrical resistivity decreased when the AZO films were annealed in the range of 200-400 ℃. The electron concentrations of the AZO films were inversely proportional to their electrical resistivities. It was also found that the electron mobility in the AZO films was proportional to their electron concentration, indicating that the conductivities of the AZO films deposited by RF-sputtering were dependent on structural imperfections such as ionized impurities and grain boundaries. Due to its detrimental effects on AZO film conductivity, O_2 mixture working gas was not used in this study.

CONFLICT OF INTEREST

The authors declare that there is no conflict of interests regarding the publication of this article.

REFERENCES

1. M. Singh and F. Scotognella, *Micromachines*, **14**, 536 (2023);
   https://doi.org/10.3390/mi14030536
2. T. Minami, *Semicond. Sci. Technol.*, **20**, S35 (2005);
   https://doi.org/10.1088/0268-1242/20/4/004
3. Z. Chen, W. Li, R. Li, Y. Zhang, G. Xu and H. Cheng, *Langmuir*, **29**, 13836 (2013);
   https://doi.org/10.1021/la4033282
4. C.I. Bright, 50 Years of Vacuum Coating Technology and the Growth of the Society of Vacuum Coaters (2007).
5. E. Fortunato, D. Ginley, H. Hosono and D.C. Paine, *MRS Bull.*, **32**, 242 (2007);
   https://doi.org/10.1557/mrs2007.29
6. H. Zhu, J. Hupkes, E. Bunte and S.M. Huang, *Appl. Surf. Sci.*, **261**, 268 (2012);
   https://doi.org/10.1016/j.apsusc.2012.07.159
7. C.H. Huang, H.L. Cheng, W.E. Chang and M.S. Wong, *J. Electrochem. Soc.*, **158**, H510 (2011);
   https://doi.org/10.1149/1.3559456
8. J.K. Wassei and R.B. Kaner, *Mater. Today*, **13**, 52 (2010);
   https://doi.org/10.1016/S1369-7021(10)70034-1
9. L. Hu, J. Song, X. Yin, Z. Su and Z. Li, *Polymers*, **12**, 145 (2020);
   https://doi.org/10.3390/polym12010145
10. G.F. Wang, X.M. Tao and R.X. Wang, *Compos. Sci. Technol.*, **68**, 2837 (2008);
    https://doi.org/10.1016/j.compscitech.2007.11.004
11. S. Sharma, S. Shriwastava, S. Kumar, K. Bhatt and C.C. Tripathi, *Opto-Electr. Rev.*, **26**, 223 (2018);
    https://doi.org/10.1016/j.opelre.2018.06.004
12. Y. Wen and J. Xu, *J. Polym. Sci. Part A: Polym. Chem.*, **55**, 1121 (2016);
    https://doi.org/10.1002/pola.28482
13. K. Ellmer, A. Klein and B. Rech, Transparent Conductive Zinc Oxide - Basics and Applications in Thin Film Solar Cells, Springer (2008).
14. M.U. Shahid, K.M. Deen, A. Ahmad, M.A. Akram and M. Aslam, *Appl. Nanosci.*, **6**, 235 (2016);
    https://doi.org/10.1007/s13204-015-0425-7
15. B.J. Babu, A. Maldonado, S. Velumani and R. Asomoza, *Mater. Sci. Eng. B*, **174**, 31 (2010);
    https://doi.org/10.1016/j.mseb.2010.03.010
16. D.C. Oh, T. Suzuki, J.J. Kim, H. Makino, T. Hanada, M.W. Cho, T. Yao and H.J. Ko, *Appl. Phys. Lett.*, **86**, 032909 (2005);
    https://doi.org/10.1063/1.1849852
17. L.Y. Chen, W.H. Chen, J.J. Wang, F.C.N. Hong and Y.K. Su, *Appl. Phys. Lett.*, **85**, 5628 (2004);
    https://doi.org/10.1063/1.1835991
18. S.H. Park, T. Minegishi, H.J. Lee, D.C. Oh, H.J. Ko, J.H. Chang and T. Yao, *J. Appl. Phys.*, **110**, 053520 (2011);
    https://doi.org/10.1063/1.3630030
19. K.B. Kim, S.M. Lee, D.C. Oh and H.-J. Ko, *J. Korean Phys. Soc.*, **67**, 676 (2015);
    https://doi.org/10.3938/jkps.67.676
20. T.S. Jang and D.C. Oh, MATEC Web of Conferences, **78**, 01106 (2016);
    https://doi.org/10.1051/matecconf/20167801106
21. D.R. Lide, CRC Handbook of Chemistry and Physics, CRC Press (2004).
22. J.F. Shackelford, Introduction to Materials Science for Engineers, MacMillian Publishing Company (1985).
23. P.J. Lin, Y.F. Lai, X.Q. Ding and S.Y. Cheng, *Chem. Eng. Trans.*, **46**, 1117 (2015);
    https://doi.org/10.3303/CET1546187
24. D.K. Kim and H.B. Kim, *J. Alloys Compd.*, **509**, 421 (2011);
    https://doi.org/10.1016/j.jallcom.2010.09.047
25. P. Gondoni, M. Ghidelli, F. Di Fonzo, V. Russo, P. Bruno, J. Marti-Rujas, C.E. Bottani, A. Li Bassi and C.S. Casari, *Thin Solid Films*, **520**, 4707 (2012);
    https://doi.org/10.1016/j.tsf.2011.10.072
26. S.I. Han and H.B. Kim, *Appl. Sci. Converg. Technol.*, **25**, 145 (2016);
    https://doi.org/10.5757/ASCT.2016.25.6.145
27. L. Lu, H. Shen, H. Zhang, F. Jiang, B. Li and L. Lin, *Optoelectron. Adv. Mater. Rapid Commun.*, **4**, 596 (2010).
28. G. Fang, D. Li and B. Yao, *Vacuum*, **68**, 363 (2002);
    https://doi.org/10.1016/S0042-207X(02)00544-4
29. D.C. Oh, S.H. Park, H. Goto, I.H. Im, M.N. Jung, J.H. Chang, T. Yao, J.S. Song, C.H. Bae, C.S. Han and K.W. Koo, *Appl. Phys. Lett.*, **95**, 151908 (2009);
    https://doi.org/10.1063/1.3247889
30. D.C. Look, Electrical Characterization of GaAs Materials and Devices, John Wiley & Sons, Chichester (1989).
31. H.E. Ruda, *J. Appl. Phys.*, **59**, 1220 (1986);
    https://doi.org/10.1063/1.336509
32. J.Y. Seto, *J. Appl. Phys.*, **46**, 5247 (1975);
    https://doi.org/10.1063/1.321593
33. G. Baccarani, B. Ricco and G. Spadini, *J. Appl. Phys.*, **49**, 5565 (1978);
    https://doi.org/10.1063/1.324477